Nanoscale

PAPER

View Article Online
View Journal | View Issue

Cite this: *Nanoscale*, 2017, **9**, 1292

SERS-enhanced piezoplasmonic graphene composite for biological and structural strain mapping†

Brandon C. Marin, Justin Liu, Eden Aklile, Armando D. Urbina, Andrew S.-C. Chiang, Natalie Lawrence, Shaochen Chen and Darren J. Lipomi*

Received 19th November 2016,
Accepted 21st December 2016

DOI: 10.1039/c6nr09005b

www.rsc.org/nanoscale

Thin-film optical strain sensors have the ability to map small deformations with spatial and temporal resolution and do not require electrical interrogation. This paper describes the use of graphene decorated with metallic nanoislands for sensing of tensile deformations of less than 0.04% with a resolution of less than 0.002%. The nanoisland-graphene composite films contain gaps between the nanoislands, which when functionalized with benzenethiolate behave as hot spots for surface-enhanced Raman scattering (SERS). Mechanical strain increases the sizes of the gaps; this increase attenuates the electric field, and thus attenuates the SERS signal. This compounded, SERS-enhanced "piezoplasmonic" effect can be quantified using a plasmonic gauge factor, and is among the most sensitive mechanical sensors of any type. Since the graphene-nanoisland films are both conductive and optically active, they permit simultaneous electrical stimulation of myoblast cells and optical detection of the strains produced by the cellular contractions.

Introduction

Piezoresistive sensors undergo a reversible change in resistance with mechanical strain and are ubiquitous in microelectromechanical systems (MEMS), wearable sensors, and structural health monitors.[1–3] Most conductive objects exhibit increased electrical resistance (R) along a strained axis simply because stretching increases the length and reduces the cross sectional area normal to the strain. The sensitivity of this modality—expressed as the gauge factor (GF = $\Delta R/\Delta\varepsilon$, where ε is the engineering strain)—for conductors with uniform composition is limited at small strains to GF = $1 + 2\nu$, where ν is the Poisson ratio.[4] Structured materials, such as thin films that rely in part on controlled fracture or quantum tunneling to mediate the resistivity, can exhibit much higher sensitivity.[5–8] Resistive sensors, however, require electrical contacts for interrogation, and can thus interfere with measurements of biophysical events that may be sensitive to small electrical potentials (*e.g.*, cell contractions).[9] In contrast, optical modes of sensing provide a route of interrogation that is in principal orthogonal to electrophysiological signals, and can do so without physical contact. The use of metallic nanoparticles on a deformable substrate offers the potential for high sensitivity for detection based on optics because of localized surface plasmons.[10,11] These surface plasmons, in turn, greatly amplify near-field signals, especially between adjacent nanoparticles that are separated by small dimensions (≤10 nm).

Our group has recently demonstrated the ability to form metallic nanoislands by physical vapor deposition on graphene using low nominal thicknesses of deposition. The morphology of the nanoisland films was controlled by exploiting the wetting transparency of graphene. That is, the surface energy of the substrate supporting the graphene influenced the morphology of the nanoisland films, and thus a wide range of morphologies could be produced, from isolated islands to percolated networks. These graphene-nanoisland composite films exhibited tunable morphologies and small gaps between adjacent nanoislands, and could be transferred to flexible substrates. In one example, we detected the contractions of mammalian cardiomyocytes using the piezoresistance of the composite films.[12] In this paper, we show that the nanoscale spacing between metallic islands permit a form of mechanical sensing based on optics. In particular, mechanical force produced by cells or other objects change the spacing between metallic nanoislands and thus modulate the electric field between them through plasmonic coupling. This effect can be augmented by adding an adsorbant to the metallic nano-

Department of NanoEngineering, University of California, San Diego, 9500 Gilman Drive, Mail Code 0448, La Jolla, CA 92093-0448, USA. E-mail: dlipomi@eng.ucsd.edu

†Electronic supplementary information (ESI) available: Finite-element simulations, finite-difference time-domain simulations, SEM micrographs, and SERS spectra. See DOI: 10.1039/c6nr09005b

islands, and measuring the surface-enhanced Raman scattering (SERS) signal of the adsorbant as a function of strain (Fig. 1). This method of sensing—a SERS-enhanced piezoplasmonic effect—provides a two-component enhancement of the signal produced by mechanical strain: first, by the strong dependence of the SERS signal on electric field, and second, by the strong dependence of the electric field on the distance of separation between the particles. The SERS-enhanced piezoplasmonic effect in principle would permit mechanical sensing that is significantly more sensitive than piezoresistive sensors.

Previous work in the area of strain-tunable optical devices, which have exploited far-field phenomena, include strain-tunable filters,[13] reflectors,[14] and gratings,[15] and dynamic color tuning.[16] Work involving near-field phenomena has included strain-tunable surface plasmon resonance,[17–20] fano resonance,[21] and strain-controlled SERS activity.[10,11,22] Although this work encompasses a wide breadth of interesting applications, strain-sensitive optical phenomena have not been used for the sensing of microscale mechanical deformations in biological systems. The use of metallic nanoislands on graphene offers a unique platform to address this challenge. These composite films permit electrical stimulation of myoblast cells with simultaneous non-contact detection of the strain produced by the cells, using a SERS-enhanced "piezoplasmonic" effect.

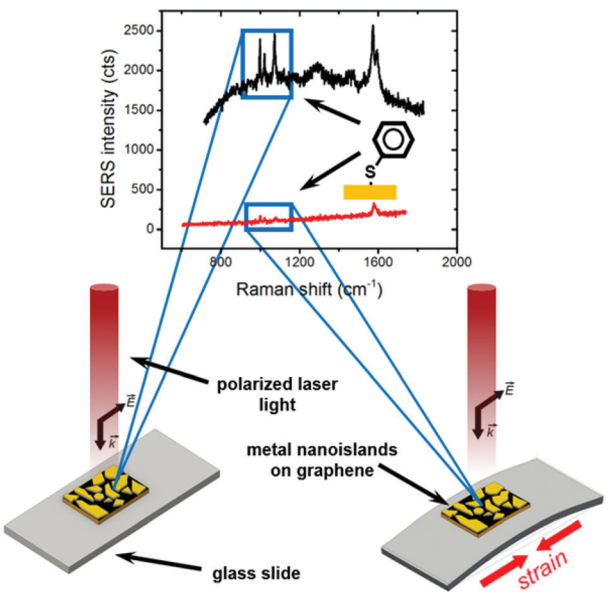

Fig. 1 Schematic diagram for strain sensing using metallic nanoislands on graphene. The metallic nanoislands have a self-assembled monolayer of benzenethiolate chemisorbed on the surface, which produced the SERS spectra shown in the diagram. The peaks in the SERS spectra corresponding to the vibrational modes of the benzenethiolate are highlighted in blue boxes. The polarization of incident laser light was in the direction of the long axis of the substrates. The substrate on the right was subjected to a bending strain, with the graphene/nanoisland film on the top surface of the bend. The tensile strain produced by bending increased the distance between the nanoislands; increased separation decreased the plasmonic coupling and thus attenuated the SERS signal.

Methods

Graphene synthesis

Graphene was synthesized using an MTI OTF-1200X-HVC-UL quartz tube furnace. Briefly, electropolished copper foil was annealed in the tube furnace at 1050 °C, 1 atm, for 30 min under flow of ultra-high purity (UHP) argon (700 SCCM) and hydrogen (60 SCCM). Following this step, graphene growth was initiated by flowing methane (0.3 SCCM), UHP argon (700 SCCM), and hydrogen (60 SCCM) into the furnace for 40 min. The methane flow was increased to 0.7 SCCM for an additional 20 min while keeping UHP argon and hydrogen flow rates constant. Hydrogen and methane flows were then terminated, which ends the synthesis. The furnace was then slow cooled to ambient temperature under UHP argon flow only.

Metal nanoisland fabrication

Metal nanoislands were fabricated by physical vapor deposition using an AJA International thermal evaporator (Orion-class). Approximately 6 nm of gold or silver was deposited onto graphene supported on copper foil at a rate of 0.05 Å s^{-1}. Chamber pressure during deposition was 2.0×10^{-7} torr. The product of this procedure was a copper foil substrate bearing a layer of graphene, and decorated with metallic nanoislands (NI/Gr/Cu). Thin films of gold or silver (100 nm) were prepared by thermal evaporation at a rate of 1 Å s^{-1} and a chamber pressure of 2.0×10^{-7} torr.

Nanoisland functionalization for SERS, substrate transfer, and testing

Benzenethiol (Sigma-Aldrich) was used as our SERS analyte. To functionalize the metal islands, a 1 mM benzenethiol ethanolic solution was prepared and drop casted onto the nanoisland side of a NI/Gr/Cu sample. Samples were allowed to incubate for 6 hours then cleaned thoroughly with ethanol and de-ionized water. To transfer nanoislands onto a substrate of interest, a water transfer method was used. The graphene was essential for this method, as it provides mechanical support for ease of transferring. To summarize for polarization studies, 200 nm of 1 kDa molecular weight poly-methylmethacrylate (PMMA) was spun (4 kRPM for 60 s) onto the functionalized nanoisland side of the NI_{func}/Gr/Cu sample, adding another layer to the sample (PMMA/NI_{func}/Gr/Cu). The backing copper foil was etched off by floating the PMMA/NI_{func}/Gr/Cu sample copper-side down on an aqueous ammonium persulfate solution (50 mg mL^{-1}). The floating island samples (now PMMA/NI_{func}/Gr) were then transferred onto a 200 μm thick glass slide for polarization studies, PMMA side up. Glass was used as a substrate to minimize the mixing of Raman signal from the substrate with the analyte (glass has a relatively low Raman signal). As a result of the substrate selection, bending strains were used to analyze the piezo response since glass cannot be effectively stretched for strain measurements. Substrates were bent and held in tension using 3D printed supports. Based on the dimensions of these supports, finite-element analysis simulations were performed to calculate the strain at the apex.

The PMMA was stripped before Raman measurements to minimize signal cross talk. Stripping was done by immersion in warm acetone (40 °C) for 30 min, followed by rinsing with isopropanol and deionized water (ambient temperature).

For cell studies, floating island samples (PMMA/NI_{func}/Gr) on water were transferred onto polymethyldisiloxane (PDMS) slabs, with the graphene side up. A diagram in Fig. S5† depicts substrate orientation in detail and the transfer process. The samples (Gr/NI_{func}/PMMA/PDMS) were then washed thoroughly with DI water, then PBS buffer solution before cell seeding.

Electron microscopy

An FEI Tecnai G2 Sphera running a LaB6 filament at 200 kV was used for transmission electron (TEM) micrographs and electron diffraction. A Gatan Ultrascan 1000 UHS CCD camera running Gatan Digital Micrograph was used for image collection. TEM samples were prepared by transferring graphene-supported nanoislands (by water-transfer method) onto unsupported 200-mesh copper TEM grids. An FEI XL30 SFEG was used for scanning-electron microscopy (SEM). Images were acquired at 15 kV accelerating voltage with a 50 μm spot and a through lens-detector. SEM samples were prepared by transferring graphene-supported nanoislands (by water-transfer method) onto silicon chips. A Hitachi HD2000 was used for combination scanning-transmission electron microscopy (STEM) running tungsten filament at 200 kV. STEM samples were prepared by transferring graphene-supported nanoislands (by water-transfer method) onto unsupported 200-mesh copper TEM grids.

Reflectance spectroscopy

Reflectance spectra were taken using a Perkin Elmer Lambda-1050 UV-vis-NIR spectrophotometer with a universal reflectance accessory (URA) module. The spectrometer acquired signal from 250–900 nm using a silicon detector with a tungsten (visible) and deuterium lamp (ultraviolet) as a source. A 1400 lines per mm holographic monochromator was used to grate the signal.

Raman spectroscopy and microscopy

All Raman spectra were collected on a Renishaw inVia Raman microscope. A 633 nm HeNe laser polarized by half-wave plates was used with an excitation power of *ca.* 1 mW. 633 nm laser light was selected due to its lower phototoxicity and higher SERS enhancement, when compared to UV-vis lasers. A 5×, 0.12 NA Leica N-Plan objective was used for both excitation and collection of Raman data. A 1800 l mm^{-1} grating was used for the dispersion of sample signal. For SERS measurements, samples were functionalized with benzenethiolate by immersion in a 1 mM ethanolic solution for 6 h, followed by rigorous cleaning in IPA and DI water. Spatially static spectra, such as those used for polar plots were collected using a 1 s acquisition at 1% laser power. Raman maps were acquired using a 3 s acquisition under 5% laser power. Map dimensions were 2100 μm × 6 μm and consisted of 1360 individual spectra. A 5-point center cumulative average was used for analysis of the SERS intensities as a function of distance from the apex. All SERS intensities for all measurements compared the intensity of the 999 cm^{-1} peak of benzenethiolate (which corresponds to vibrational mode 12 in Wilson notation).[23] This vibrational mode was particularly chosen due to the isotropic nature of its Raman tensor, which prevented any bias in polarization measurements.[24]

Finite-difference time domain (FDTD) simulations

2D FDTD electromagnetic simulations were performed using Lumerical FDTD solutions with a mesh size of 2 Å. Palik dielectric data was used for silver and gold. Falkovsky dielectric data was used for graphene. Geometries for metal nanoislands were based on TEM images (Fig. S3†). Simulations were performed at an incident wavelength of 633 nm, the excitation wavelength of the laser used for Raman spectroscopy. The incident light was polarized and coherent.

Finite-element simulations of glass

Autodesk Inventor was used to simulate bent glass (50.8 mm × 19.05 mm × 0.20 mm) through finite-element analysis. The strain along the length of the slide as a function of distance from apex was calculated after applying 54 N, 124 N, and 203 N of force to the center, with the maximal strain occurring at the apex with values of 0.032, 0.074, and 0.12 percent strain, respectively. Force was applied from the bottom with the two end of the glass held by immobile contacts. Deformation analysis using FEA assumes linear, static stress that is proportional to load applied, linear material properties and neglects yielding and buckling.

Myoblast cell (C2C12) culture, maintenance and characterization

C3H/C2C12 murine myoblast cells were purchased from ATCC and cultured according to protocol provided by ATCC. C2C12 cells were cultured in Dulbecco's Modified Eagle Medium (DMEM, Gibco) supplemented with 10% fetal bovine serum, heat inactivated (Hyclone), and 1% penicillin/streptomycin (Gibco). Cells were maintained in a 37 °C incubator with 5% CO_2. C2C12 cells were differentiated by culturing in DMEM with 5% horse serum and 1% penicillin/streptomycin for 3 days. Cells were treated with 0.25% trypsin EDTA (Gibco) and were then seeded onto the graphene side of the silver nanoisland substrate (Fig. S5†) at a density of 3000 cells per mm^2. Cells were cultured for at least 3 days before analysis.

Cells were fixed with 4% paraformaldehyde (PFA, Life Technologies) in phosphate buffered saline for 15 min, washed 3 times for 5 min in phosphate buffer solution (PBS, 100 mM NaCl, 8.0 pH). Cells were permeabilized using and blocked using 2% (wt/vol) bovine serum albumin and 0.1% (wt/vol) Triton-X100 (Sigma-Aldrich) in PBS for 1 h. Samples were washed 3 times in PBS for 5 minutes. Cells were counterstained with myosin heavy chain (rabbit) primary antibody (1 : 100, Sigma) in PBS with 2% BSA overnight. Samples were washed 3 times with PBS for 5 min and following primary

incubation, they were incubated with FITC-Phallodin (1 : 100, Life Technologies), donkey anti-rabbit 543 (1 : 200, Biotium) and Hoescht 33258 for nuclei (1 : 2000, Invitrogen). Finally, samples were imaged at 40× using a Leica DMI6000 inverted fluorescence microscope.

For SEM micrographs, cells were fixed with 4% PFA for 15 minutes and dehydrated using a gradient of 20%, 50%, 60%, 70%, 80%, 90%, 95%, and 100% ethanol incubations at room temperature. Samples were incubated in 20% ethanol for 20 min and subsequent dehydration steps were 5 minutes each. Samples were dried using a Touisimis Critical Point Drier and were then coated with iridium by DC sputtering. SEM micrographs were acquired using an FEI XL30 SFEG, as previously described.

For electrical cell stimulation, nanoisland samples were electrically addressed with eutectic gallium indium (EGaIn). Samples were then pulsed with 5-volts, at 2 Hz, with a square wave profile, using a Siglent SDG2042X function/arbitrary waveform generator.

Results and discussion

In order to determine usefulness as a SERS substrate, we characterized the morphologies and optical properties of silver and gold nanoislands. The transmission electron microscope (TEM) images for gold (Fig. 2a) and silver (Fig. 2b) nanoislands suspended on single-layer graphene show small gaps between the nanostructures, which appear as lighter regions. These gaps are highly active for SERS, due to the strong electric fields present in plasmonic coupling of noble metal interfaces.[25–27] The optical response of the nanoislands lies in the visible range (Fig. 2c and d). Plasmon resonance contributes to stronger absorption of light for nanoislands relative to their thin-film counterparts as compared for gold and silver in Fig. 2c and d, respctively. This plasmon resonance and its associated electric field (E) are crucial to the sensitivity of an optical strain gauge. The magnitude of E in coupled plasmonic modes over small length scales is believed to vary between d^{-3} and d^{-6}, where d is the separation between plasmonic nanoparticles.[28,29] The electromagnetic SERS effect of chemical species located in the gaps between metallic nanoparticles, in turn, varies with E^4. The compounding nonlinear effects of (1) the dependence of the gap size on electric field and (2) the dependence of SERS effect on the magnitude of the electric field resulted in a piezoplasmonic effect that exhibited remarkable sensitivity in the low strain regime.

To quantify the effect of strain on the SERS intensity, we functionalized metal nanoislands on graphene films with a self-assembled monolayer (SAM) of benzenethiolate. We then transferred the films bearing nanoislands to thin (200 μm) glass slides. These slides could be deformed easily by loading them into brackets fabricated by 3D printing. The tensile strains on the top surfaces of the slides were calculated by finite-element modeling (Fig. S1†). Large bending radii produced small tensile strains. In this small-strain regime (<0.2%), the nanoislands exhibited an anisotropic response in the SERS signal based on the polarization of incident light (Fig. 3a). That is, the SERS signal of the benzenethiolate SAM was diminished when light was polarized parallel to the direction of strain. This result was consistent with increased spacing between the gaps along the strained axis, *i.e.*, that nanoislands were being pulled apart.

We observed that the difference between the SERS signal of a benzenthiolate SAM in response to polarization between the strained and unstrained axis increased with increasing strain. This increased anisotropy in the signal was consistent with strain-induced separation between nanoislands supporting the SAM; increased separation produced a larger contrast in SERS intensity between light polarized in the direction of strain and

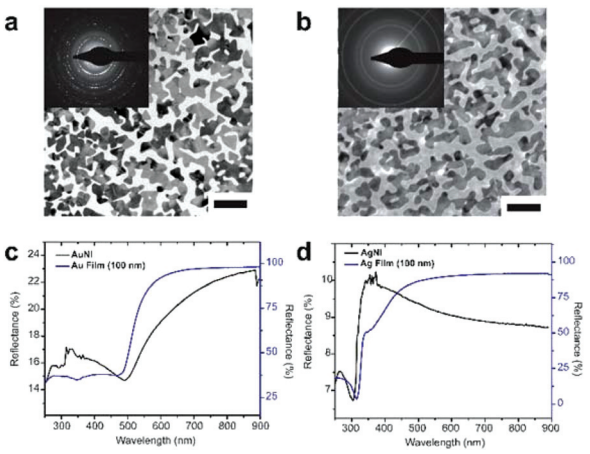

Fig. 2 Morphology and optical spectra of nanoislands on graphene. Transmission electron micrographs (TEM) and electron diffraction patterns (insets) of gold nanoislands (AuNI, a) and silver nanoislands (AgNI, b) to provide a comparison on crystallinity. Scale bars, 100 nm. Reflectance spectra of gold (c) and silver (d) nanoislands with spectra of unstructured, continuous 100 nm metal films for comparison. The dips in reflectance of gold are lower in energy than those of silver because of unequal relativistic contractions between the two metals.

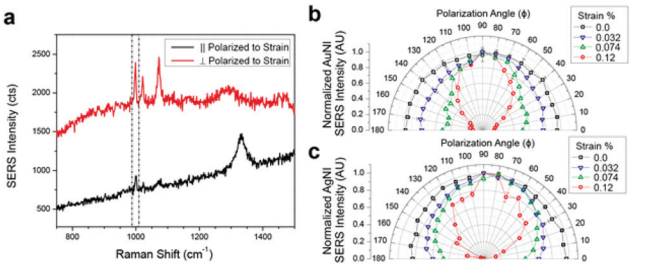

Fig. 3 Polarization response of nanoislands under strain. (a) SERS spectra of gold nanoislands under 0.074% strain with incident laser light polarized parallel and perpendicular to strain. The peak of interest in chemisorbed benzenethiol is highlighted between the dashed lines (999 cm^{-1} peak). Radial plots of gold (b) and silver (c) nanoislands, which reveal the polarization response of the SERS signal with the graphene-nanoisland film under strain. The radial plots are normalized to maximum SERS intensity of the peak indicated in panel (a).

orthogonally (Fig. 3a). (We note that the anisotropy in response to polarization was greater for silver nanoislands than it was for gold, as see in Fig. 3b and c.) Essentially, strain changes the size of gaps between nanoislands and the nature of surface plasmons confined between them. Non-linear decay of the SERS signal with respect to separation is consistent with the results of others.[29–31]

In analogy to the gauge factor (GF) used for piezoresistive sensors to quantify the response to strain,[4] we propose a plasmonic gauge factor ($GF_{plasmonic}$), which quantifies the SERS response of films of metallic nanoparticles to strain,

$$GF_{plasmonic} = \frac{\frac{I_{unstrained} - I_{strained}}{I_{strained}}}{\varepsilon}$$

where $I_{unstrained}$ and $I_{strained}$ are defined as the SERS intensities of unstrained and strained films, respectively, with the incident polarization held constant (in the direction of the long axis of the slide). A high sensitivity is indicated by large contrasts between $I_{strained}$ (which should decrease as nanoislands are pulled apart) and $I_{unstrained}$, which yields a high $GF_{plasmonic}$. Fig. 4 plots $GF_{plasmonic}$ as a function of strain for silver and gold nanoislands. Silver nanoislands demonstrated a more sensitive piezoplasmonic response based on $GF_{plasmonic}$ values, especially at the lowest strains tested (~0.03%). Compared to gold, silver has the ability to confine stronger electric fields in nanostructures.[32,33] To reinforce this observation, we performed finite-difference time domain (FDTD) simulations of gaps between silver nanoislands and gold nanoislands to determine the electric field profile at the Raman laser wavelength (633 nm). Our FDTD results (Fig. S2†) confirm that gaps between silver nanoislands have a higher magnitude of E than do gaps between gold nanoislands. A comparison of $GF_{plasmonic}$ between the responses of gold and silver nanoislands is shown in Fig. 4.

One of the advantages of detecting strain using a contiguous optically active film is the ability to measure gradients of deformation. To demonstrate this ability, we obtained polarization-dependent maps of the SERS intensity of a graphene/silver nanoisland film located near the apex of a rectangular glass slide under a small bending radius. The bending deformation produced a strain gradient along the long axis, with the greatest strain (0.032%) located at the apex (Fig. S1 and Table S1†). Fig. 5a shows a bright field image comprising 12 individual micrographs of the gradient, with the apex of the bent substrate indicated by the dotted line. The dimensions of the long and narrow rectangular region were 2100 μm × 6 μm (the raw 2D spectral images are shown in Fig. S4†), which is marked by the yellow line in Fig. 5a. When incident light was polarized in the direction of the strain gradient (0° with respect to the x-axis), a clear decrease in SERS signal could be detected (Fig. 5b). The SERS signal was lowest at the area of highest strain (the apex). As the polarization was increased to 45° (Fig. 5b), the gradient in SERS signal was diminished, as the nanoislands were separated along the long axis. With polarization 90° to the axis of the strain gradient (Fig. 5b), we observed little variation in the SERS signal. According to finite-element simulations (Table S1†), the gradient in SERS intensity in the narrow rectangular region corresponded to a total range in strain of 0.0017%.

Since the graphene-nanoisland films are both electrically conductive and optically active, we tested their ability to be used in an optoelectronic biosensing platform. That is, the electrical conductivity of graphene could be used for stimulation of a strain-producing biophysical event and strain-dependent SERS could be used for detection of the deformation. To test this hypothesis, we measured the SERS spectrum of the electrically-induced strain response of myoblast

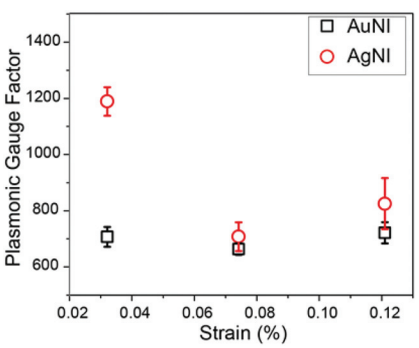

Fig. 4 Piezoplasmonic characterization of noble metal nanoislands. Plasmonic gauge factors of gold nanoislands (AuNI) and silver nanoislands (AgNI) are plotted as a function of strain.

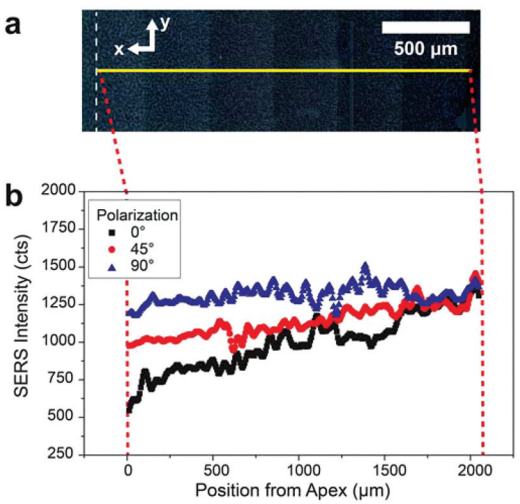

Fig. 5 SERS mapping of strain gradients using a bent glass substrate bearing silver nanoislands on graphene. (a) Bright-field image of silver nanoislands on a bent glass substrate (scale bar, 500 μm). The yellow line near the center of the image is the selected area (2100 μm × 6 μm) that was mapped using a Raman microscope. The apex of the bent substrate is marked by the dotted white lines and has a strain of 0.032%. (b) A moving average of the SERS intensity along the x-axis in the selected area under three different polarizations (0°, 45°, and 90° in respect to the x-axis). Note that the signal decreases as the polarization aligns with the principle direction of deformation (x-direction).

(C2C12) cells grown on silver nanoisland substrates to determine if the stimulated contraction could be detected optically through changes in the SERS signal. Silver nanoislands supported by graphene functionalized with benzenethiolate were transferred onto PDMS with the graphene-side up to maintain biocompatibility (Fig. S5†). The C2C12 cells were then grown, differentiated, and seeded on the substrates, which were then electrically addressed with droplets of a liquid metal, eutectic gallium–indium (EGaIn). The area on the sample from which the SERS signal was collected is indicated by the black box in Fig. 6a. Fig. 6b shows scanning electron microscope (SEM) images that were taken of C2C12 cells dehydrated using critical point drying (CPD) to demonstrate that the cells were interacting with the substrate. To investigate the structure of the C2C12 cells, fluorescence images of the adherent cells were taken one day after seeding. Fig. 6c clearly shows the individually labeled nuclei (blue), actin (green), and myosin heavy chain (red) in the cells.

The samples were illuminated with 633 nm laser light to collect the SERS signal. Without any voltage, the SERS signal remained constant, as depicted in Fig. 6d. A pulsed voltage (2 Hz, 5 V square-wave) was then applied to induce the differentiated C2C12 cells to contract. The periods of time during which the voltage was applied are indicated by the gray areas in Fig. 6d. A clear decrease in SERS intensity is observed under pulsed voltage, which was repeatable as indicated in Fig. 6d.

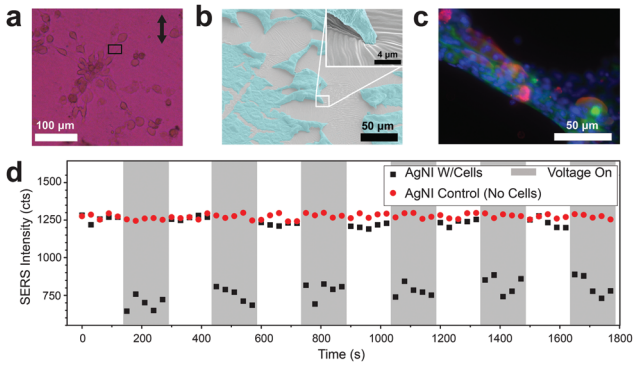

Fig. 6 Optical detection of strain induced by electrical stimulation of C2C12 myoblast cells supported by a substrate consisting of silver nanoislands on graphene. (a) A bright-field image of C2C12 cells on the substrate, with the incident polarization of the Raman laser indicated by the black arrow. The area of illumination by the Raman laser is indicated by the black box. (b) Scanning electron micrographs of critical-point dried C2C12 cells on the substrate demonstrate the interaction of the cells with the underlying nanoislands substrate. Note the stretch marks on the substrate caused by strain. Cells were false colored blue in the micrograph. (c) A fluorescence image of C2C12 cells on the substrate with nuclei (blue), actin (green), and myosin heavy chain (red) clearly visible. (d) The SERS intensity of benzenethiolate chemisorbed to silver nanoislands in the illumination area is depicted as a function of time. The gray areas indicate time periods when the C2C12 cells were stimulated by a pulsed voltage, causing them to contract and pull silver nanoislands apart which translated to a decreased SERS signal (black squares). As a control, silver nanoislands without cells were also stimulated by pulsed voltage (red circles).

This decrease in intensity suggested that the separation between the silver nanoislands was increasing due to the stress transferred to the substrate by contraction of the C2C12 cells. The area selected for illumination was a region that encompassed the border of two C2C12 cells. We hypothesized that as the cells contracted under voltage, the underlying silver nanoislands were pulled apart; this change in geometry caused a decrease in plasmonic coupling, thus leading to a decreased signal. As a control, silver nanoisland substrates without cells were pulsed under voltage to determine if the effect was based on an unknown piezoelectric effect (contraction or expansion under electrical stimulus) in the metal nanoislands. As depicted in Fig. 6d, silver nanoislands without cells exhibited no change in signal when stimulated with a pulsed voltage. The SERS spectra of the substrates was dominated by the benzenethiolate signal (Fig. S6†), which suggested that the majority of the signal came from small volume confined to the gaps between the nanoislands, *i.e.*, hotspots. Considering the myriad of organic species present in the vicinity of the nanoislands—*e.g.*, graphene, cells, PDMS, and media solution—capable of producing unwanted SERS signals (SERS crosstalk), the high signal-to-noise ratio for benzenethiolate was gratifying. (Ordinarily, SERS crosstalk can make it difficult to extract information of interest in complex biological systems.[34,35])

Conclusions

A SERS-enhanced piezoplasmonic effect can be used to detect small strains, gradients of strain, and a non-contact method of measuring the electrically induced contractions of myoblast cells. By exploiting the fact that the electric field produced by surface plasmons between adjacent metal structures changes dramatically—coupled with the strong dependence of the SERS effect on electric field—we were able to detect strains as low as 0.032% with a resolution of less than 0.002%. The small strain regime is well suited for a piezoplasmonic sensor, as the most significant responses occur over small length scales. Although piezoresistive sensors offer excellent response over a wide range of strains,[6,36] a piezoplasmonic sensor offers high sensitivity over small strain regimes. Moreover, metallic nanoislands on graphene offer a simple approach to fabricating SERS-based strain sensors that are easily transferrable onto to nearly any substrate. These sensors can be used to measure both the magnitude and spatial distribution of strain. In considering implementation of a technology such as this over large areas, nanoislands can be fabricated without the need for costly lithographic techniques. That is, the SERS-active substrates form automatically on graphene without the need for e-beam lithography or self-assembly. We believe, however, that the most compelling attributes of graphene-supported nanoislands as optical strain sensors is the spatial resolution (for strain mapping) and orthogonality of electrical stimulation and optical interrogation, which holds promise for high-throughput measurement of cellular electrophysiology.

Acknowledgements

This work was supported by the National Institutes of Health Director's New Innovator Award, grant 1DP2EB022358-01 to D. J. L., and by a Diversity Supplement (for B. C. M.) under the same award number. A. S.-C. C. was supported by the UC LEADS program, and E. A. received partial support from the CA-NASA/UCSD Space Grant Consortium. J. L. and S. C. are supported in part by California Institute for Regenerative Medicine (RT3-07899) and National Institutes of Health (R01EB021857). This work was performed in part at the San Diego Nanotechnology Infrastructure (SDNI), a member of the National Nanotechnology Coordinated Infrastructure, which is supported by the National Science Foundation (Grant ECCS-1542148). B. C. M. would like to acknowledge the use of the Cryo-Electron Microscopy Facility at UC San Diego which is supported by NIH grants to Dr. Timothy S. Baker, Dr. James Bouwer, and a gift from the Agouron Institute. The authors acknowledge Prof. Andrea R. Tao for use of the Renishaw Raman Spectrometer which was purchased with a DURIP Grant (N000141310655).

Notes and references

1 M. Li, H. X. Tang and M. L. Roukes, *Nat. Nanotechnol.*, 2007, **2**, 114.
2 X. Liu, M. Mwangi, X. Li, M. O'Brien and G. M. Whitesides, *Lab Chip*, 2011, **11**, 2189.
3 M. Pacelli, L. Caldani and R. Paradiso, Annu. Int. Conf. IEEE Eng. Med. Biol. Proc., 2006, 5358.
4 W. P. Mason and R. N. Thurston, *J. Acoust. Soc. Am.*, 1957, **29**, 1096.
5 M. Segev-Bar, A. Landman, M. Nir-Shapira, G. Shuster and H. Haick, *ACS Appl. Mater. Interfaces*, 2013, **5**, 5531.
6 L. Yi, W. Jiao, K. Wu, L. Qian, X. Yu, Q. Xia, K. Mao, S. Yuan, S. Wang and Y. Jiang, *Nano Res.*, 2015, **8**, 2978.
7 D. H. Ho, Q. Sun, S. Y. Kim, J. T. Han, D. H. Kim and J. H. Cho, *Adv. Mater.*, 2016, **28**, 2601.
8 N. Hu, Y. Karube, C. Yan, Z. Masuda and H. Fukunaga, *Acta Mater.*, 2008, **56**, 2929.
9 H. Bayley and C. R. Martin, *Chem. Rev.*, 2000, **100**, 2575.
10 M. K. Hossain, G. R. Willmott, P. G. Etchegoin, R. J. Blaikie and J. L. Tallon, *Nanoscale*, 2013, **5**, 8945.
11 H. Kang, C. J. Heo, H. C. Jeon, S. Y. Lee and S. M. Yang, *ACS Appl. Mater. Interfaces*, 2013, **5**, 4569.
12 A. V. Zaretski, S. E. Root, A. Savchenko, E. Molokanova, A. D. Printz, L. Jibril, G. Arya, M. Mercola and D. J. Lipomi, *Nano Lett.*, 2016, **16**, 1375.
13 N. T. Huang, S. C. Truxal, Y. C. Tung, A. Hsiao, S. Takayama and K. Kurabayashi, *Appl. Phys. Lett.*, 2009, **95**, 2.
14 K. Kim, J. Seo and M. Oh, *Opt. Express*, 2008, **16**, 1423.
15 S. C. Truxal, K. Kurabayashi and Y.-C. Tung, *Int. J. Optomechatronics*, 2008, **2**, 75.
16 H. Fudouzi and T. Sawada, *Langmuir*, 2006, **22**, 1365.
17 S. Olcum, A. Kocabas, G. Ertas, A. Atalar and A. Aydinli, *Opt. Express*, 2009, **17**, 2051.
18 F. Huang and J. J. Baumberg, *Nano Lett.*, 2010, **10**, 1787.
19 X. Qian and H. S. Park, *J. Mech. Phys. Solids*, 2010, **58**, 330.
20 W. Wu, M. Ren, B. Pi, Y. Wu, W. Cai and J. Xu, *Appl. Phys. Lett.*, 2015, **107**, 18.
21 Y. Cui, J. Zhou, V. A. Tamma and W. Park, *ACS Nano*, 2012, **6**, 2385.
22 E. B. Wilson, *Phys. Rev.*, 1934, **45**, 706.
23 E. Le Ru and P. Etchegoin, *Principles of Surface-Enhanced Raman Spectroscopy: And Related Plasmonic Effects*, Elsevier, Oxford, 2008.
24 K. D. Alexander, K. Skinner, S. Zhang, H. Wei and R. Lopez, *Nano Lett.*, 2010, **10**, 4488.
25 S. Eustis and M. A. El-Sayed, *Chem. Soc. Rev.*, 2006, **35**, 209.
26 P. L. Stiles, J. A. Dieringer, N. C. Shah and R. P. Van Duyne, *Annu. Rev. Anal. Chem.*, 2008, **1**, 601.
27 Y. Zhao, X. Li, Y. Du, G. Chen, Y. Qu, J. Jiang and Y. Zhu, *Nanoscale*, 2014, **6**, 11112.
28 S. A. Maier, P. G. Kik, H. A. Atwater, S. Meltzer, A. A. G. Requicha and B. E. Koel, *Proc. SPIE. – Int. Soc. Opt. Eng.*, 2002, **4810**, 71.
29 X. Zhang, J. Zhao, A. V. Whitney, J. W. Elam and R. P. Van Duyne, *J. Am. Chem. Soc.*, 2006, **128**, 10304.
30 P. K. Jain, W. Huang and M. A. El-Sayed, *Nano Lett.*, 2007, **7**, 2080.
31 K. A. Willets and R. P. Van Duyne, *Annu. Rev. Phys. Chem.*, 2007, **58**, 267.
32 K.-S. Lee and M. A. El-Sayed, *J. Phys. Chem. B*, 2006, **110**, 19220.
33 C. J. Orendorff, L. Gearheart, N. R. Jana and C. J. Murphy, *Phys. Chem. Chem. Phys.*, 2006, **8**, 165.
34 R. A. Tripp, R. A. Dluhy and Y. Zhao, *Nano Today*, 2008, **3**, 31.
35 M. D. Porter, R. J. Lipert, L. M. Siperko, G. Wang and R. Narayanan, *Chem. Soc. Rev.*, 2008, **37**, 1001.
36 N. M. Sangeetha, N. Decorde, B. Viallet, G. Viau and L. Ressier, *J. Phys. Chem. C*, 2013, **117**, 1935.